

Original Research Paper

In silico and *in vitro* Structural Analysis on the Interaction of Calmodulin and Calmodulin-Binding Motif of FKBP35 from *Plasmodium knowlesi*

¹Sazlinawatie Aladin, ^{1,2}Cahyo Budiman, ²Muhamad Arifin and ¹Rafida Razali

¹Biotechnology Research Institute, Universiti Malaysia Sabah, Kota Kinabalu, Sabah, Malaysia

²Department of Animal Production and Technology, Faculty of Animal Sciences, IPB University, Bogor, Indonesia

Article history

Received: 15-08-2024

Revised: 05-12-2024

Accepted: 20-12-2024

Corresponding Author:

Cahyo Budiman

Biotechnology Research Institute,

University Malaysia Sabah, Kota

Kinabalu, Sabah, Malaysia

Email: cahyo82@gmail.com

Abstract: FK506-binding protein 35 (FKBP35) is a peptidyl-prolyl cis-trans isomerase found in *Plasmodium knowlesi*, a zoonotic malaria parasite responsible for concerning cases of malaria infection in East Malaysia. This protein contains a segment known as the calmodulin-binding motif (Pk-CBM), which is predicted to facilitate interaction with calmodulin from *P. knowlesi* (Pk-CaM). Although this interaction is considered promising for future antimalarial drug development, it has not yet been experimentally demonstrated. This study aims to investigate the binding between the Pk-CBM of FKBP35 and Pk-CaM through both *in silico* and *in vitro* approaches, with a focus on the structural features of this interaction. To address this, three-dimensional models of Pk-CaM and Pk-CBM were first constructed using SWISS-MODEL, and the docking complex was generated using HADDOCK. Subsequently, MD simulations were carried out using the YASARA structure package to assess the stability of the interaction over a period of 100 ns, utilizing the AMBER14 force field under conditions of 298 K (25°C) and pH 7.4 in an explicit water environment. Furthermore, to confirm the *in silico* binding event, an *in vitro* experiment was conducted to assess the binding between Pk-FKBP35 and the CBM using circular dichroism and anilinonaphthalene-1-sulfonic acid (ANS) fluorescence assays. The docking simulation revealed that the C-terminal segment of Pk-CBM, particularly the IL motif, is essential for binding to Pk-CaM, with detailed mapping of residue-specific interactions provided by LigPlot. These computational results were corroborated by *in vitro* studies, which demonstrated that the binding event significantly altered the secondary structure of Pk-CaM and involved its hydrophobic regions. Together, these findings confirm a significant interaction between Pk-CaM and Pk-CBM, suggesting potential novel druggable targets for antimalarial drug design aimed at *P. knowlesi*.

Keywords: Malaria, *Plasmodium knowlesi*, FKBP35, Molecular Docking, Molecular Dynamics Simulation, Circular Dichroism, Fluorescence

Introduction

Malaria is recognized as a global health concern. In 2021, it is estimated that there were 247 million cases of malaria worldwide, spanning 84 malaria-endemic countries, including the territory of French Guiana. This represents a 2 million increase in cases compared to the previous year, 2020 (World Health Organization, 2022). Human malaria parasites consist of *Plasmodium falciparum* (*P. falciparum*), *Plasmodium vivax* (*P. vivax*),

Plasmodium malariae (*P. malariae*) and *Plasmodium ovale* (*P. ovale*). Additionally, a fifth species called *Plasmodium knowlesi* (*P. knowlesi*) is still classified as a zoonosis and responsible for several cases in Southeast Asia (Millar and Cox-Singh, 2015).

In Malaysia, there has been a decline in overall malaria cases; however, there has been a concerning increase in infections caused by *P. knowlesi*, especially among individuals engaged in agriculture or residing in forested areas (Chin *et al.*, 2020). *P. knowlesi* primarily infects

long-tailed (*Macaca fascicularis*) and pig-tailed macaques (*M. nemestrina*), serving as their main natural hosts (Huff *et al.*, 1972). The rapid replication of *P. knowlesi* poses challenges as it affects both humans and monkeys, and its resemblance to other types of malaria complicates diagnosis and treatment. Furthermore, these parasites exhibit adaptability and resistance, hindering effective treatment (Singh and Daneshvar, 2013).

Several strains of *P. falciparum* and *P. vivax* were reported to have gained resistance towards this drug, but such instances remain unknown among the *P. knowlesi* strains (Goh *et al.*, 2018). While the current state of *P. knowlesi* treatment indicates no resistance to antimalarials, it is crucial to continue researching new therapeutic candidates. Multiple strains of *Plasmodium* species, including those that are resistant to antimalarials, are increasingly emerging in Southeast Asian countries. Therefore, the exploration of alternative treatment options remains necessary to effectively address potential future challenges posed by drug-resistant strains (Amir *et al.*, 2018).

There have been recent reports indicating that an immunosuppressant drug, FK506 (tacrolimus), demonstrates antimalarial activity, and no cases of drug resistance have been documented thus far (Monaghan *et al.*, 2017; Goh *et al.*, 2018). Although FK506 demonstrates antimalarial properties, its prolonged use as an antimalarial drug is not feasible or preferable due to its potential immunosuppressive effects on patients. Consequently, it is essential to investigate alternative compounds that can serve as antimalarial drugs in replacing FK506 without compromising the immune system and without promoting drug resistance (Monaghan *et al.*, 2005).

FK506 drug is effective in suppressing the immune system by binding and inhibiting the FK506-Binding Protein (FKBP), as a member of peptidyl-prolyl cis-trans isomerase of the parasites, which in turn hinders the activation of T-cells (Tung, 2010; Budiman *et al.*, 2011). Studies have reported that the FKBP35 parasites protein interacts with FK506, demonstrating PPIase activity towards tetrapeptide substrates, functioning as a chaperone, and inhibiting the phosphatase activity of calcineurin with or without the presence of FK506 (Monaghan and Bell, 2005; Yoon *et al.*, 2007). Goh *et al.* (2018) indicated that the functional roles of FKBP35 in parasite cells include assisting in protein synthesis, particularly for cis-proline-containing proteins, preventing protein aggregation through its chaperone activity, and mediating calcium signaling pathways through calcineurin activity. Monaghan and Bell (2005) suggested that these cumulative functional roles contribute to the pathogenesis of the malaria parasite.

Studies of FKBP35 from *P. falciparum* and *P. knowlesi*, designated as Pf- and Pk-FKBP35, by Yoon *et al.* (2007); Goh *et al.* (2018), indicated that the proteins

organized into two distinct functional domains of the FK506-Binding Domain (FKBD) and the tetratricopeptide-repeat domain (TPRD). While FKBD serves as the catalytic site, the TPRD, on the other hand, has no role on catalytic activity and serve as the dimerization site. Earlier, Pk-FKBP35 was reported to play a crucial role in facilitating cis-prolyl bond-containing proteins and preventing protein aggregation (Silvester *et al.*, 2017; Goh *et al.*, 2018; Illang *et al.*, 2023). As a result, Pk-FKBP35 represents a promising target for the development of drugs to combat *P. knowlesi* infection. Another study conducted on FK506-binding protein 35 (FKBP35) in *Plasmodium falciparum* reported the existence of A Calmodulin-Binding Motif segment (CBM) within its TPR domain (Alag *et al.*, 2009; Yoon *et al.*, 2007). Similarly, Silvester *et al.* (2017) observed the presence of a CBM segment of Pk-FKBP35 (designated as Pk-CBM in this study) at the C-terminal region, which is also part of its TPR domains which this segment extended from Val260-Ala302. The existence of this segment suggests that Pk-FKBP35 is capable of binding to calmodulin in *P. knowlesi* (Pk-CaM) and may participate in calcium-mediated cellular signaling pathways. This, nevertheless, has never been experimentally evidenced. It is important to note that the essential roles of calmodulin in the pathogenesis of malaria parasites are widely reported. Calmodulin modulates calcium signaling pathways, which in turn regulate the effector molecules involved in parasite motility, invasion, development, and egress (de Oliveira *et al.*, 2021).

It is widely reported that many proteins containing CBM indeed exhibited binding to calmodulin, in which the CBM segment acts as a recognition site for calmodulin. In this respect, CBM segments often contain the unique IQ motif, although variations in the sequence have been observed, with a few conserved amino acids, particularly I and Q, being common in most IQ motifs (Bähler and Rhoads, 2002). However, Pk-CBM does not contain the IQ motif; instead, it has IR and IL motifs. Similar variations in the IQ motif have been reported by Rhoads and Friedberg (1997), where not all proteins have canonical IQ motifs but still retain the ability to bind to calmodulin. These observations raise questions regarding whether the binding of Pk-CBM is not solely determined by the canonical IQ motif. It also suggests the possibility that the IR and IL motifs may play a similar role as IQ motifs in calmodulin binding. Hypothetically, Pk-CaM may bind to Pk-CBM through its IR or IL motif. Accordingly, the current study attempted to investigate the binding interaction between Pk-CBM and Pk-CaM, identifying the motifs critical for this interaction through both *in silico* and *in vitro* analyses. The findings contribute to the potential discovery of antagonistic molecules that disrupt the interaction between FKBP35 and calmodulin, ultimately leading to the death of the malaria parasite by disrupting its calcium signaling pathway.

Materials and Methods

Protein 3D Structure Prediction and Model Validation of Pk-CaM and Pk-CBM

The DNA sequence of Pk-CaM was obtained from the PlasmDB database (transcript ID: PKNH_0420800.1). The DNA sequence was then converted to protein sequences using the online server ExPasy Translate (Mollazadeh *et al.*, 2022). Meanwhile, the Pk-CBM sequence was obtained from the Pk-FKBP35 validated model by Silvester *et al.* (2017). The tertiary structures of Pk-CaM and Pk-CBM were generated using SWISS-MODEL (Biasini *et al.*, 2014). The selection of the best model was based on the latest version of Qualitative Model Energy Analysis (QMEAN), called QMEANDisCo (Studer *et al.*, 2020). The Pk-CaM model was then evaluated and validated using the PROCHECK server (Laskowski *et al.*, 1993) according to the Ramachandran values (Lovell *et al.*, 2003), Verify3D score (Lüthy *et al.*, 1992) and G-factor (Aslanzadeh and Ghaderian, 2012). The best model is then saved as a .pdb format file for further Analysis. As for the Pk-CBM model, it is validated using the Molprobit score, clash score, Ramachandran favored (%), Ramachandran outlier (%), and Rotamer outliers (%) (Chen *et al.*, 2012). Additionally, Pk-CBM variants were also being generated using SWISS-MODEL, as designated as:

- VAR 1: Pk-CBM sequence without IL motif
- VAR 2: Pk-CBM sequence without IR motif
- VAR 3: Pk-CBM sequence by changing IL motif into ND motif
- VAR 4: Pk-CBM sequence by changing IR motif into NA motif

Molecular Docking Between Pk-CBM and Pk-CaM

Molecular docking is used to predict the interaction between the receptor and ligand using the High Ambiguity Driven protein-protein DOCKing (HADDOCK) server (Kumari *et al.*, 2022; Dominguez *et al.*, 2003). The receptor is calmodulin from *P. knowlesi* (Pk-CaM) and the ligand will be the Pk-CBM and its variants, which were obtained from the previous step in .pdb format files. The multi-docking server combines these AIRs to generate docked complexes for CaM-CBM. HADDOCK configuration parameters are set to defaults. Initially, HADDOCK generates 1000 models, and the best 200 structures are selected based on energy. In the second iteration, a simulated annealing protocol is performed. The resulting structures are then clustered according to their HADDOCK scores, taking into account their refined explicit solvents. Subsequently, 10 models are chosen based on the lowest HADDOCK score and Z score after cluster-structural Analysis. The docking complexes are

then evaluated based on the HADDOCK score. The best complex is chosen for further Analysis and saved as a .pdb file. The complex is designated as:

- CaM-CBM: Docking complex between Pk-CaM with wild type Pk-CBM
- CaM-VAR 1: Docking complex between Pk-CaM with VAR 1
- CaM-VAR 2: Docking complex between Pk-CaM with VAR 2
- CaM-VAR 3: Docking complex between Pk-CaM with VAR 3
- CaM-VAR 4: Docking complex between Pk-CaM with VAR 4

Then, all complexes binding affinities, ΔG (kcal mol⁻¹), and dissociation constant, K_d (M), were calculated using PRODIGY (<https://wenmr.science.uu.nl/prodigy/>).

Three-Dimension Representation of Ligand, Receptor and Docking Complex

The 3D model of Pk-CaM in its Apo-form (as the receptor) and Pk-CBM with its variants (as the ligand), as well as the best docking complex, were visualized using BIOVIA Discovery Studio Visualizer for three-dimension representation (Kumar *et al.*, 2020).

Molecular Dynamic Simulation of the Complexes

Molecular Dynamic (MD) simulation was performed using YASARA Dynamics v. 20.8.1, according to Siraj *et al.* (2021), to validate the stability of the protein complex. The simulation performed using the YASARA structure package determined the structural stability of the CaM-CBM complex. The simulation was carried out at 298 K (25°C), pH 7.4, in an explicit water environment, employing an AMBER14 force field, periodic cell boundary condition, and constant pressure. Initially, the solvated structure underwent 15,000 steps of minimization using the steepest descent method at a temperature of 298 K and constant pressure. Subsequently, the complex underwent a two ns equilibration period. Following equilibration, a production MD was conducted for 100 ns under constant temperature and pressure.

Interaction Analysis of the Complexes

The docking complex will be analyzed by LigPlot v 1.4.5 (Laskowski and Swindells, 2011). The interactions between Pk-CaM and Pk-CBM, along with their variants, will be analyzed using DimPlot in LigPlot software.

In vitro Binding Analysis

1. Preparation of Recombinant Pk-CaM

Recombinant Pk-CaM was prepared by overexpressing the protein in *Escherichia coli*

BL21(DE3) as described by Robert *et al.* (2023). For this purpose, *E. coli* BL21(DE3) cells harboring a pET28a plasmid containing the Pk-CaM gene were cultured in Luria-Bertani (LB) broth at 37°C. Protein expression was induced by adding 1 mM IPTG (isopropyl β-D-1-thiogalactopyranoside) and cells were incubated at 20°C overnight post-induction. Following harvest, the cells were disrupted on ice using sonication, and the protein was purified using Ni-NTA affinity chromatography. Protein purity was assessed by SDS-PAGE (15%) using the method of Laemmli (1970).

2. Pk-CBM Peptide Synthesis

The peptide sequence corresponding to Pk-CBM was derived from the full sequence of Pk-FKBP35, as described by Silvester *et al.* (2017), and used to synthesize Pk-CBM peptide. This sequence spans from Val260 to Lys302. The peptide was then chemically synthesized by Shanghai RoyoBiotech Co., Ltd., with a purity greater than 95%. No modifications were introduced to the synthetic Pk-CBM peptide.

3. Circular Dichroism Spectroscopy

Circular Dichroism (CD) analysis was conducted to assess secondary structural changes in Pk-CaM upon binding with the Pk-CBM peptide, both with and without calcium ions. Far-UV CD spectra of Pk-CaM were analyzed under conditions with and without Pk-CBM, following the protocols outlined by Budiman *et al.* (2009) and Au *et al.* (2023). Recombinant Pk-CaM was prepared in a 20 mM sodium phosphate buffer (pH 8.0) containing 2 mM CaCl₂ and incubated at 25°C for 30 min prior to Analysis. For far-UV CD measurements (200-260 nm), Pk-CaM was used at a concentration of approximately 0.2 mg/mL, and data were collected using a 2 mm path length cuvette. Pk-CBM was added to Pk-CaM in concentrations ranging from 0-50 μM. The dissociation constant (K_d) was calculated by plotting changes in the relative CD signal at 220 nm against Pk-CBM concentrations, using a single binding-site affinity model under the equation $Y = \frac{B_{max} \cdot X}{K_d + X}$, where Y , B_{max} , X , and K_d are the specific binding, the concentration of ligand, and the dissociation constant, respectively.

4. ANS Fluorescence Spectroscopy

The method for measuring ANS binding to Calmodulin (CaM) with the CBM peptide was based on the approach described by Jensen *et al.* (2015), with modifications. A solution containing five μM CaM, 50 μM ANS (1-anilinonaphthalene 8-sulfonate), two mM CaCl₂, and varying concentrations of the Pk-CBM peptide was prepared. The sample was excited at 345 nm and the emitted fluorescence was recorded using a Plate Reader Infinite 200 PRO, with measurements taken across wavelengths from 400-650 nm. The average fluorescence

lifetime was calculated from the fitted data to assess the binding interactions between Pk-CaM and Pk-CBM, using ANS as a fluorescent probe.

Data Analysis

All non-structural data were analyzed descriptively following the methods of Kia *et al.* (2015), Adiyoga *et al.* (2022), and Afiyah *et al.* (2015). Structural data were analyzed based on relevant statistical parameters, following the approaches of Silvester *et al.* (2017) and Lindang *et al.* (2022). The parameters for obtaining the best structural models were QMean, PROCHECK, and Ramachandran Plot. QMEAN uses statistical potentials of mean force to generate global and per-residue quality estimates (Waterhouse *et al.*, 2018). The PROCHECK program computes a number of stereochemical parameters for the given protein model and compares them with 'ideal' values obtained from a database of well-refined high-resolution protein structures in the Protein Data Bank (Laskowski *et al.*, 2012). The Ramachandran plot shows the statistical distribution of the combinations of the backbone dihedral angles φ and ψ (Park *et al.*, 2023). Meanwhile, statistical parameters in docking and molecular dynamic simulations rely on the Z score and RMSD. The graph obtained from CD spectra and ANS fluorescence was generated from 10 cycles of measurements.

Results

Protein 3D Structure Prediction and Model Validation of Pk-CaM and Pk-CBM

The Pk-CaM protein sequence converted using ExPasy translate was MADKLTEEQISEFKEAFSLFDKDGDTITTKELGTVMRSLGQNPTEAELQDMINEIDTDGNGTIDFPEFLTLMARKMKDSTDTEELIEAFRVFDRDGDGYISADELRHVMTNLGEKLTNEEVDEMIREADIDGDGQINYEEFVKMMIAK. Pk-CBM protein sequence was VEIRNSYDMCLNKLKEARKRDKLTFFGGMFDKGLYEEKKSSAK.

The 3D models for Pk-CaM and Pk-CBM were generated using the SWISS-MODEL serve and then evaluated using QMEANDisco. QMEAN employs statistical potentials of mean force to estimate the quality of protein structures on both global and local scales, considering various structural features and statistical information. QMEANDisCo, the latest version of QMEAN, improves the accuracy of local quality estimates by assessing the consistency of observed interatomic distances in the protein model with ensemble information from experimentally determined homologous protein structures. By incorporating this additional information, QMEANDisCo enhances the reliability and accuracy of its quality estimates, particularly at the local

level. A QMEANDisCo value close to 1 indicates high trustworthiness (Studer *et al.*, 2020). Among all the models generated using SWISS-MODEL for Pk-CaM, Model 1 had the highest value QMEANDisCo which was 0.79 ± 0.07 . Thus, this QMEANDisCo value is used for choosing the best model for further validation.

The evaluation of stereochemical and geometric aspects of the tertiary structure using the PROCHECK server was used for PK-CaM Model 1, indicating that most residues (94.7%) were in the most favorable regions (Q and y values), while 5.3% of residues were in allowed regions. None of the residues were found in generously allowed or disallowed regions. Additionally, the overall average G-factor of dihedral angles and main-chain covalent forces for Model 1 was -0.10 , surpassing the acceptable cut-off of -0.5 . The G-factor provides a measure of the plausibility of a stereochemical property, and a higher G-factor implies a higher conformational probability (Aslanzadeh and Ghaderian, 2012). Furthermore, the Verify 3D score for Model 1 (93.88%) exceeded the requirement ($>80\%$), indicating the correctness of the model (Lüthy *et al.*, 1992). This score evaluates segments of the model based on how well the residues' environments (e.g., burial, secondary structure) align with their observed tendencies for being in those environments. Therefore, Model 1 meets the criteria to be the most suitable model for further Analysis of Pk-CaM and is saved as a .pdb file. The three-dimensional representation for Model 1 Pk-CaM using BIOVIA Discovery Studio Visualizer is shown in Fig. (1).

Pk-CBM and its variants 3D model were generated using SWISS-MODEL shown in Table (1) and Fig. (2) and saved as a .pdb file.

Table 1: Evaluation and validation of the generated structural quality of Pk-CBM and its variants

Model	Pk-CBM (wild type)	VAR 1	VAR 2	VAR 3	VAR 4
QMEANDisCo	0.68 ± 0.1	0.48 ± 0.1	0.52 ± 0.1	0.47 ± 0.1	0.56 ± 0.1
Molprobit score	1.36	1.12	1.39	1.04	0.59
Clash score	0	0	0	0	0
Ramachandran	90.24	87.18	89.74	90.24	97.56
Favored (%)					
Ramachandran outliers (%)	2.44	5.13	2.56	2.44	0
Rotamer outliers (%)	2.63	0	2.78	0	0

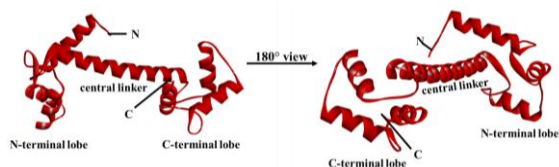


Fig. 1: 3D model for Pk-CaM (Model 1)

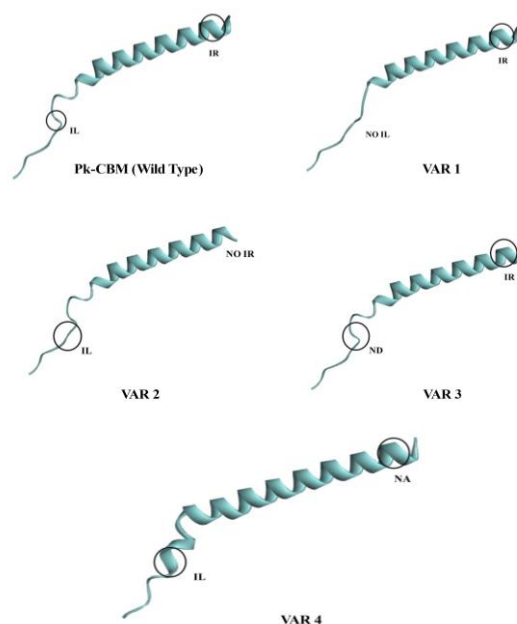


Fig. 2: 3D model for Pk-CBM and its variants

Molecular Docking Between Pk-CaM and Pk-CBM

Molecular docking was performed using HADDOCK for Pk-CaM and Pk-CBM (wild type) with the model obtained from the previous step. HADDOCK clustered 18 structures into 9 clusters, representing 9% of the water-refined models generated. Statistical Analysis of the top ten clusters was conducted for the docking analysis of Pk-CaM and Pk-CBM (wild type), resulting in the CaM-CBM complex. For the docking of Pk-CaM with VAR 1, HADDOCK clustered 28 structures into 12 clusters, representing 14% of the water-refined models generated. Among the top 10 clusters, the best CaM-VAR 1 complex was chosen. For the docking between Pk-CaM with VAR 2, HADDOCK clustered six structures into 3 clusters, representing 3% of the water-refined models generated. The best docking model was named the CaM- VAR 2 complex. In the docking of Pk-CaM with VAR 3, HADDOCK clustered 19 structures into 9 clusters, representing 9% of the water-refined models generated. The best complex was chosen and named, CaM-VAR 3. For the docking between Pk-CaM with VAR 4, HADDOCK clustered 26 structures into 12 clusters, representing 13% of the water-refined models generated. The best complex was named CaM-VAR 4. All complexes were selected based on the lowest HADDOCK score and Z score, as shown in Table (2). The binding affinities, ΔG (kcal mol⁻¹), and dissociation constant, K_d (M), were calculated using PRODIGY, as shown in Table (3). The three-dimensional representation of the best docking complex is shown in Fig. (3).

Table 2: The best models from HADDOCK docking between Pk-CBM and its variants with Pk-CaM

Model	CaM-CBM	CaM-VAR 1	CaM-VAR 2	CaM-VAR 3	CaM-VAR 4
HADDOCK Score	-77.0±0.4	-72.3±7.4	-47.0±2.8	-86.5±5.2	-76.5±10.6
RMSD	18.4±0.2	16.2±0.5	18.1±0.4	27.7±0.1	27.2±0.2
Van der Waals energy	-20.5±9.6	-9.0±0.9	-16.4±6.6	-12.9±2.3	-0.0±0.8
Electrostatic energy	-234.9±66.8	-373.7±56.3	-105.7±37.9	-410.0±1.2	-428.4±42.7
Desolvation energy	-9.5±4.1	11.5±4.8	-9.5±3.8	8.4±2.6	9.2±2.8
Restraints violation energy	0	0	0	0	0
Buried Surface Area	1312.6±144.3	842.9±128.2	661.1±74.8	1040.7±36.5	953.8±167.2
Z-score	-1.9	-2.6	-1.3	-2.2	-2.0

Table 3: Binding affinities and dissociation constant of HADDOCK docking models

Model	CaM-CBM	CaM-Var 1	CaM-Var 2	CaM-Var 3	CaM-Var 4
Binding affinities, ΔG (kcal mol ⁻¹)	-6.2	-8	-5.4	-6.8	-5.3
Dissociation constant, K_d (M)	0.000028	0.0000013	0.00001	0.000011	0.000012

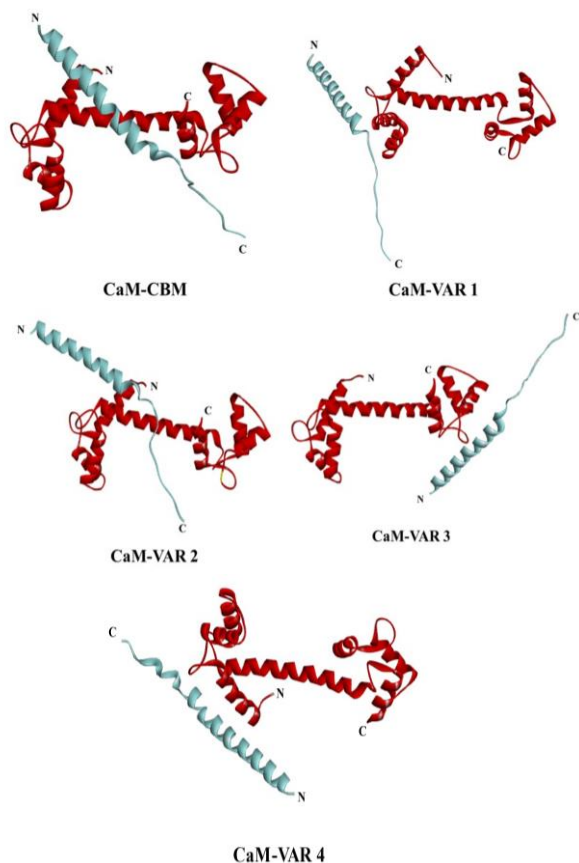


Fig. 3: HADDOCK docking model between Pk-CBM and its variants with Pk-CaM

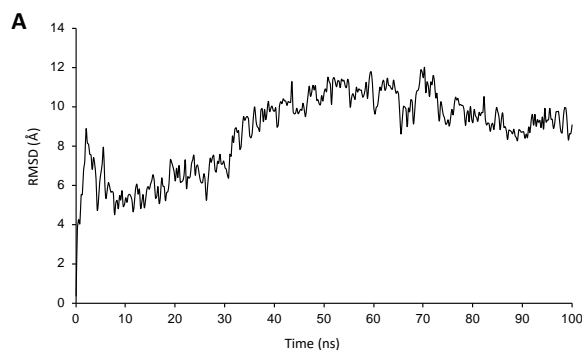
Molecular Dynamic Simulation of CaM-CBM Complex

The molecular dynamics simulation performed on the CaM-CBM complex using the YASARA program, which generated a graph for Root Mean Square Deviation (RMSD) (Fig. 4A), Radius of gyration (Rg) (Fig. 4B), and Root Mean Square Fluctuation (RMSF) (Fig. 4C).

The Root Mean Square Deviation (RMSD) analysis of the CaM-CBM complex (Fig. 4A) initially exhibits significant fluctuations, with RMSD values reaching up to 4 Å, indicating structural adjustments and flexibility in the early stages. Around the 45 ns mark, the complex begins to stabilize, as reflected in a reduction in RMSD fluctuations. Beyond this point, the RMSD values show a gradual decrease, suggesting that the complex is moving toward a more stable and equilibrated conformation. This trend implies that, after an initial period of adjustment, the CaM-CBM complex maintains its structural integrity more consistently, indicating the establishment of a stable interaction under the simulation conditions.

The radius of gyration (Rg) graph shown in Fig. (4B) illustrates the changes in Rg values over time, which begin to stabilize at approximately six ns of simulation time. Throughout the simulation, the Rg values for all the complexes remained relatively stable, exhibiting only minor deviations of 1-2 Å. This indicates that the overall compactness or size of the complexes remained consistent and did not undergo significant conformational changes.

The RMSF analysis was performed to assess the movement and fluctuation of residues in the Pk-CaM protein complex. The results are shown in Fig. (4C), where the RMSF values for residues involved in hydrogen bond interactions, such as Arg75 (1.98 Å), Asp79 (2.11 Å) and Glu140 (2.86 Å), were found to be around 2 Å. Similarly, residues involved in hydrophobic interactions, including Met147 (2.74 Å), Lys144 (2.51 Å), Asn138 (2.82 Å) and Tyr139 (2.71 Å), also exhibited RMSF values close to 2 Å. Some residues, like Asp134 (3.85 Å), showed RMSF values exceeding 3 Å. Similarly, residues involved in hydrophobic interactions, such as Asp3 (5.81 Å), Val131 (3.86 Å), and Asp132 (4.22 Å), also had higher RMSF values.



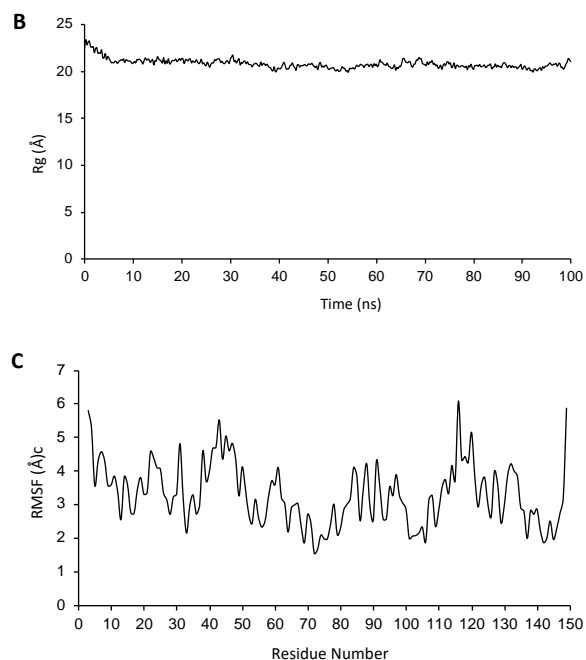


Fig. 4: (A) RMSD values; (B) Rg values; and (C) RMSF values of the complex during simulation under YASARA

Interaction Analysis

The interaction map among the residues in the complexes were further analyzed, as shown in Fig. (5). The interaction map of the wild-type Pk-CBM and Pk-CaM reveals both hydrogen bond and hydrophobic interactions are critical for the stability of the complex. Specifically, ionic interaction is observed between Lys39(B) from Pk-CBM and Asp134(A) from Pk-CaM. While hydrogen bonds interaction was observed between Asp21(B) and Arg75(A), Arg20(B) and Asp79(A) at a distance of 2.70 Å as well as Leu34(B) and Glu140(A) at a distance of 2.65 Å. These interactions help stabilize the complex through specific residue pairings.

In addition to these hydrogen bonds, several hydrophobic interactions are also identified, including Phe29(B), Ala17(B), Leu14(B), Ile33(B), and Tyr35(B) from Pk-CBM, which interact with Met147(A), Lys144(A), Asp3(A), Val131(A), Asp132(A), Asn138(A) and Tyr139(A) from Pk-CaM. These hydrophobic contacts further reinforce the structural integrity of the complex, promoting a tightly packed interface between the two subunits. Together, these interactions are essential for maintaining the conformation and functionality of the CaM-CBM complex.

Key residues of the IL motif involved in the interaction include Ile 33(B), which forms hydrogen bonds, and Leu 34 (B), which participates in hydrophobic interactions, both of which play critical roles in stabilizing the complex. Other essential residues in this interaction include Leu14, Ala17, Arg20, Asp21, Phe29, Tyr35, and Lys39.

In the CaM-VAR 1 complex (Fig. 5B), Lys31(B) forms an interaction with Asp51(A) at a distance of 2.67 Å, contributing to the overall stability of the protein. Lys22(B) interacts with several residues from chain A, including Asp25(A), forming ionic interaction and form hydrogen bond interaction with Cys27(A), Glu32(A), and Asp23(A) at a distance of 2.92 Å, 2.65 Å, 2.66 Å, that reinforce the structural integrity of the complex. Additionally, Lys15(B) forms interactions with both Asp23(A) with 2 interactions at a distance of 2.73 and 2.52 Å and Gly24(A) at a distance of 2.67 Å, further promoting structural cohesion. Another hydrogen bond interaction where Met28(B) interacts with Gln50(A) at a distance of 2.94 Å, likely forming a hydrophobic contact that helps stabilize the interface. These interactions are crucial for the stability and function of the CaM-VAR 1 complex, with salt bridges and hydrogen bonds playing key roles in maintaining the protein's conformation. The hydrophobic interactions involving residues such as Phe29(B), Gly26(B), Gly27(B), Leu23(B), Lys19(B), Asn54(A), Gly62(A), Asn61(A), Thr63(A) and Thr29(A), further enhance the complex's stability by promoting a tightly packed, energetically favorable interface between the subunits. These combined interactions facilitate the proper folding and functional activity of the complex, which is essential for its biological role.

For the CaM-VAR 2 complex (Fig. 5C), where the IR motif is removed, the residues involved are Phe27 (B) form a hydrogen bond with Lys78 (A) at a distance of 3.08 Å, while Lys29 (B) forms hydrogen bonds with Arg 75 (A) at distances of 2.87 Å and 2.92 Å. In addition to these hydrogen bonds, hydrophobic interactions are observed between several residues from both proteins. Specifically, Asn71, Asp3, Ala58 and Asp79 of Pk-CaM interact hydrophobically with Phe23, Ile31, Tyr33 and Gly30 of VAR 2.

In the CaM-VAR 3 complex (Fig. 5D), where the IR motif is substituted with the ND motif, it reveals that Lys 22 (B) forms hydrogen bonds with Ile126 (A), Gly135 (A), and Asp130 (A) at distances of 2.76 Å, 2.81 Å and 2.55 Å, respectively. Additionally, Arg18 (B) forms a hydrogen bond with Asp96 (A) at a distance of 2.58 Å, and Lys15 (B) forms hydrogen bonds with Asp134 (A) and Gln136 (A) at distances of 2.68 Å and 2.78 Å, respectively. Ionic interactions are also observed, with Lys19 (B) interacting with Asp134 (A) and Lys15 (B) interacting with Asp132 (A). Moreover, hydrophobic interactions are seen between Phe29 and Leu11 from VAR 3 residues and Glu120, Asn98, and Ser102 of Pk-CaM residues.

Finally, in the CaM-VAR 4 complex (Fig. 5E), where the IR motif is replaced by the NA motif, reveals that Lys38 (B) forms hydrogen bonds with Asp25 (A) and Asp23 (A) at distances of 2.59 Å and 2.56 Å, respectively. Additionally, Lys15 (B) forms a hydrogen bond with Asp8 (A) at a distance of 2.58 Å, and Arg18 (B) forms

hydrogen bonds with Glu12 (A) at distances of 2.61 Å and 2.62 Å. Furthermore, Lys22 (B) forms a hydrogen bond with Lys14 (A) at a distance of 2.76 Å. Ionic interactions are observed with Lys22 (B) interacting with Asp7 (A). Hydrophobic interactions are seen between Leu34, Gly26, Phe25, Phe29, and Tyr35 of VAR 4 residues and Gly26 and Cys27 of Pk-CaM residues.

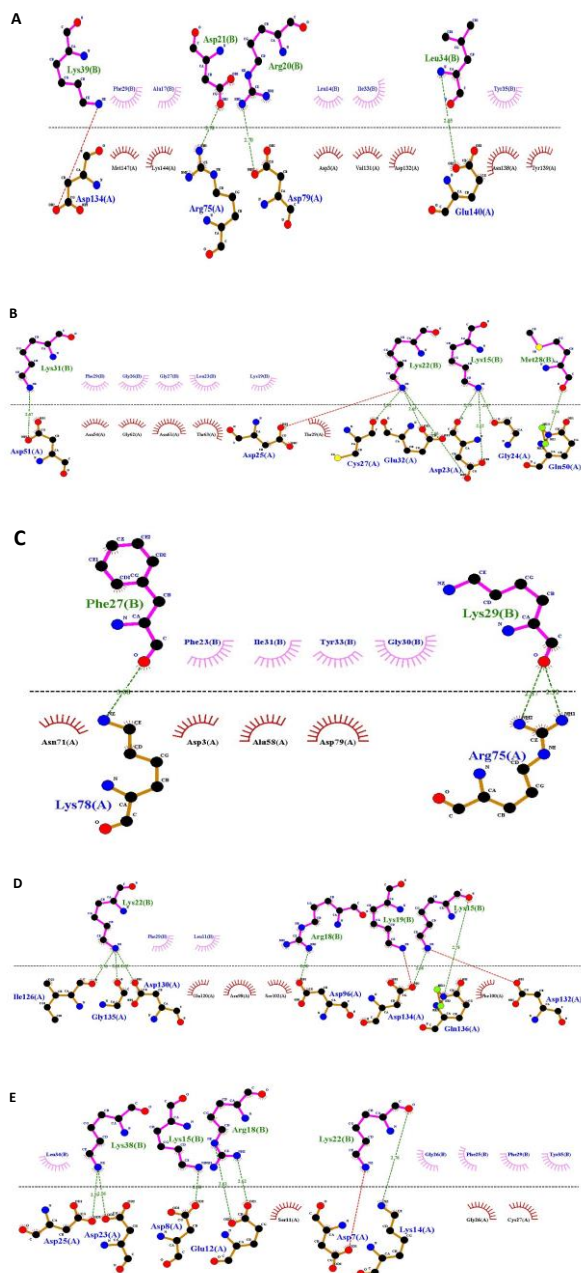


Fig. 5: Interaction map of the complexes of (A) CaM-CBM, (B) CaM-VAR 1, (C) CaM-VAR 2, (D) CaM-VAR 3, (E) CaM-VAR 4, complex generated using Dimplot from LigPlot+ Software. The residues of Pk-CaM (the receptor) and Pk-CBM, or its variants as the receptor, were shown at the bottom and upper parts of the map, respectively

In vitro Analysis

E. coli BL21(DE3) (Novagen Inc., Madison, WI, USA) was used as a host strain for the overproduction of N-terminal His-tagged forms of full-length Pk-CaM as it was widely used for recombinant protein expression. In addition, we have also successfully produced recombinant malaria proteins using this host cell (Goh *et al.*, 2018; Illang *et al.*, 2023). Protein preparation involved expressing all proteins in soluble form within *E. coli* cells during overproduction, yielding a single band on SDS-PAGE (Fig. 6), with an apparent size of about 21 kDa. This size corresponds to the theoretical size derived from the amino acid sequence, with the addition of a 6His-tag. In a previous study, Robert *et al.* (2023) also reported successful expression and purification of Pk-CaM using an *E. coli* host system, obtaining a similar apparent size following a single purification step using Ni-NTA affinity chromatography. The yield of Pk-CaM protein from the current purification of a 1 L culture ranged from 8-10 mg of purified protein. Robert *et al.* (2023) further indicated that the recombinant Pk-CaM expressed in *E. coli* retained its functionality, exhibiting calcium ion binding activity comparable to that of the native protein.

CD Spectra Binding Analysis

CD spectra were performed to assess changes in the secondary structure of Pk-CaM upon binding with its calmodulin-binding motif (Pk-CBM). As shown in Fig. (7A), Pk-CaM exhibited distinct alterations in its CD spectral profile following the addition of Pk-CBM, indicative of changes in its α -helical content. These spectral changes suggest that the binding of Pk-CBM induces structural rearrangements in Pk-CaM's secondary structure. Additionally, Fig. (7B) illustrates the relationship between the CD signal and increasing concentrations of Pk-CBM. A progressive decrease in the CD signal was observed with higher Pk-CBM concentrations, pointing to a concentration-dependent interaction between Pk-CaM and Pk-CBM. The plot fitted into a single binding-site affinity model, which allows the calculation of the dissociation constant (Kd) to be 54.8 μ M. Fig. (7A) showed a comparison between the fluorescence emission of ANS with Pk-CaM alone and Pk-CaM in the presence of CBM, further confirming that CBM binding results in a significant reduction in ANS fluorescence. These changes might be indicated the binding event between both molecules indeed occurred.

ANS Fluorescence Spectroscopy

Further, the fluorescence emission spectra of ANS in the presence of Pk-CaM were also measured at varying concentrations of CBM peptide (Fig. 8A). In the absence of CBM (0 μ M), a strong fluorescence intensity was observed with a peak around 450-500 nm, indicating significant binding of ANS to the hydrophobic regions of Pk-CaM, which were fully exposed in the absence of Pk-

CBM. However, upon the addition of Pk-CBM, a marked decrease in fluorescence intensity was observed, suggesting that the Pk-CBM peptide interacts with Pk-CaM and likely occupies or alters its hydrophobic sites, thereby reducing the binding of ANS. The reduction of ANS signal in Fig. (8B) implied a dose-dependent decrease in ANS fluorescence intensity as the concentration of Pk-CBM increased, supporting the hypothesis that Pk-CBM competes with ANS for the same hydrophobic binding sites on Pk-CaM. This progressive reduction in fluorescence indicates that Pk-CBM binding to Pk-CaM leads to a displacement of ANS.

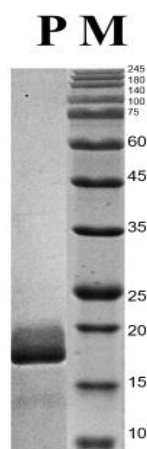


Fig. 6: SDS-PAGE of purified recombinant Pk-CaM. Lane M and P refer to protein markers for sizing references (kDa) and Pk-CaM samples, respectively. The band corresponding to Pk-CaM is indicated by the arrow.

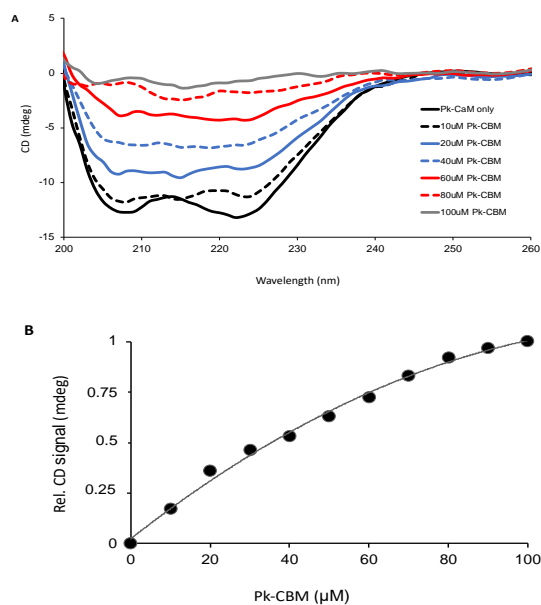


Fig. 7: (A) Changes of secondary structure upon Pk-CaM and Pk-CBM binding using CD spectroscopy; (B) Relationship CD signal against Pk-CBM at different concentration

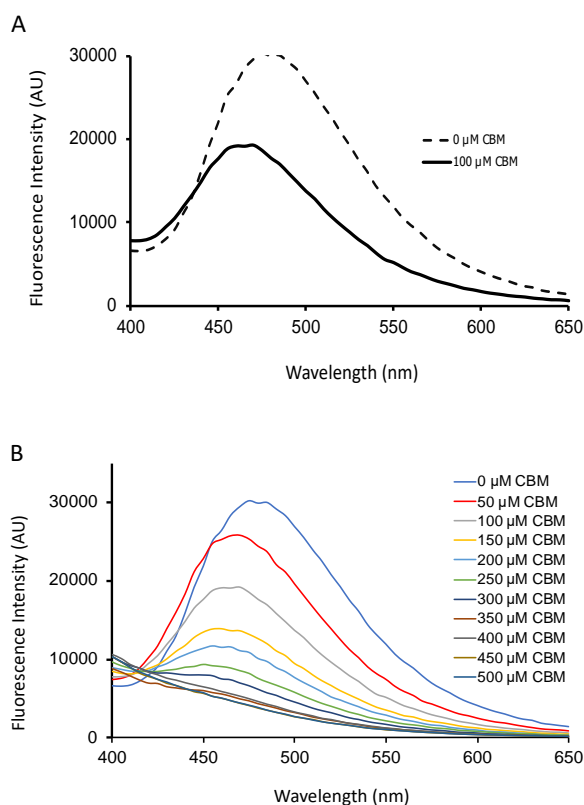


Fig. 8: Fluorescence emission spectra of ANS in the presence of Pk-CaM (A) with varying Pk-CBM peptide concentrations and (B) comparing conditions with and without the Pk-CBM

Discussion

An earlier study by LaCount *et al.* (2005) emphasized that the pathogenesis of malaria relies on intricate protein-protein interactions within parasite cells. In this context, the recent discovery of a Calmodulin-Binding Motif (CBM) segment in *Plasmodium* FKBP35 points to the potential for a functional interaction network between calmodulin (CaM) and FKBP35. Such an interaction could play a crucial role in supporting parasite cell processes. This study provides significant evidence confirming this interaction, advancing our understanding of the molecular mechanisms underlying malaria pathogenesis. The interaction was first investigated through *in silico* Analysis through docking simulation. For this purpose, the structural homology model of Pk-CaM was constructed, which revealed its canonical structure of calmodulin, which is dominated by helical segments. The presence of N- and C-terminal domains was well observed in the model, which is believed to harbor EF-hand motifs that bind to calcium ions. These EF-hand motifs are characterized by a typical Helix-Loop-Helix (HLH) configuration (Andrews *et al.*, 2020).

In addition, Pk-CBM (wild type and the variants) was also constructed, which all assume helical structures. These structures were comparable to a previous findings by Silvester *et al.* (2007), highlighting the complete helical structure of the CBM segment of Pk-CBM. The variants of Pk-CBM constructed in this study were built by changing the IL or IR motif. As the variant structures closely resemble the WT Pk-CBM, it is believed that the IR or IL motif has no serious contribution to the structural properties of Pk-CBM. It is plausible since the changes are only on a few residues and, therefore, unlikely to have a significant impact on the structure. Earlier, Budiman *et al.* (2012) also indicated that point mutations on the proteins, in many cases, had no effect on the structure.

Further, the model of Pk-CaM with Pk-CBM and its variants were docked using HADDOCK. The best models obtained and analyzed in this study were considered to be reliable by referring to the HADDOCK scores. The score predicted better quality and stronger binding affinity compared to other models within each cluster, according to the HADDOCK scoring system (Kumari *et al.*, 2022). The HADDOCK score provides an overall energy assessment; however, it is still a computational prediction and may not always perfectly correlate with experimental observations. Based on a comparison of different parameters, all docking models exhibit better overall performance in several aspects, including a low RMSD value, which indicates a close fit with the experimental or reference structure (Dominguez *et al.*, 2003). Additionally, the selected models showed lower intermolecular energies among the clusters, which include Van der Waals energy, electrostatic energy, desolvation energy, and restraints violation energy. A higher buried surface area was also observed, suggesting an extensive protein-protein interaction interface, which is generally considered favorable (Dominguez *et al.*, 2003). Furthermore, all models had a Z-score that reflected good agreement between predicted and expected energy values for native complexes. The Z-score measures the deviation, in terms of standard deviations, between the HADDOCK score of a specific cluster and the average score of all clusters. A lower Z-score signifies a better result, indicating greater separation from the mean score (Van Zundert *et al.*, 2016). These findings emphasize the promising characteristics of all docked models, warranting further investigation for their potential in protein-protein docking studies.

As shown in Fig. (3), the spatial orientation of Pk-CBM differs significantly from that of the other variants. In Pk-CBM, the N-lobe and the lobe-linker segment of Pk-CaM contribute to the binding. However, modification or replacement of the IR or IL motif in Pk-CBM alters this orientation. Based on Fig. (3), all four variants are accommodated only by the N-lobe of Pk-CaM, which may suggest that the affinity of these variants differs from that of Pk-CBM. The role of CaM lobes in protein

interactions has been widely reported (Dürvanger *et al.*, 2023; Horváth *et al.*, 2005; Zhang *et al.*, 2012). Notably, Dürvanger *et al.* (2023) showed that, in addition to the lobe regions, the lobe-linker region in the calmodulin-protein complex provides an additional "grip" that strengthens the interaction. Therefore, the interaction between Pk-CaM and the wild-type Pk-CBM is believed to be the most favorable due to the involvement of this linker region. However, the HADDOCK score and binding affinity data (Tables 2-3) suggest that the Pk-CaM and Pk-CBM complex does not exhibit the highest score or affinity. This does not imply that the variant's interaction with Pk-CaM is superior to that of the wild-type Pk-CBM; rather, it indicates that alterations in the IR or IL motifs of CBM indeed change its binding properties. Additionally, a stronger affinity does not necessarily indicate a more favorable interaction. In some cases, binding occurs at an incorrect site, leading to a non-functional interaction between the molecules.

While the docking yielded a reliable model from the HADDOCK platform, it remains a question of whether the complex is stable. Accordingly, MD simulation was performed to investigate the Pk-CaM and Pk-CBM models or their variants. The simulation indicated the complex begins to show signs of stabilization at approximately 45 ns, as shown by the RMSD graph. Prior to this point, the complex experienced substantial fluctuations in RMSD, with deviations of less than 4 Å. The RMSD illustrates how the protein structure deviates from a reference structure, offering information on structural changes as the simulation progresses (Cheng and Ivanov, 2012). As the simulation progresses beyond the initial fluctuations, the RMSD values gradually decrease, indicating a trend toward a more stable state. The complex ultimately achieves an overall stable configuration, with the RMSD values consistently lower by approximately 4 Å compared to the initial fluctuation range. The ability of the complex to maintain a lower RMSD value after the initial fluctuations suggests a more favorable and well-defined conformation.

In Fig. (4B), the stable Rg values suggest that the complexes maintained their structural integrity and did not experience substantial expansion or contraction. The limited deviation observed in the Rg values further indicates that the complexes maintained a relatively uniform and well-defined conformation during the simulation (Swargiary *et al.*, 2022). The consistent Rg values provide confidence in the reliability of the simulations and suggest that the complexes were structurally well-behaved throughout the study.

RMSF quantifies the movement of a group of atoms compared to their average positions during a simulation, indicating the degree of fluctuation or deviation from the average structure throughout the entire simulation (Cheng and Ivanov, 2012). The RMSF values of the interacting residues of Pk-CaM are shown in Fig. (4C).

Based on hydrogen bond interactions, the RMSF value is around 2 Å. Meanwhile, other residues involved in hydrophobic interactions also show RMSF values around 2 Å. An RMSF value range of 1-3 Å is considered acceptable for a protein to be considered structurally stable (Parikesit and Nurdiansyah, 2021). Note that some residues involved in hydrogen bond interactions have RMSF values exceeding 3 Å, such as Asp 134 (3.85 Å). This is acceptable since these residues are located near the loop region of Pk-CaM. Similarly, residues involved in hydrophobic interactions with RMSF values higher than 3 Å are due to the inherent flexibility of the loop region, which is considered acceptable and does not indicate protein complex instability. Cheng and Ivanov (2012) noted that RMSF serves as an indicator of the flexibility of different regions of a protein, which can be correlated with crystallographic B factors.

The interaction map of the CaM-CBM complex (Fig. 5A) highlights a network of interactions predominantly driven by hydrophobic contacts, as shown by the pink curved lines linking various residues. These hydrophobic interactions play a key role in stabilizing the binding interface through nonpolar contacts, which minimize the exposure of hydrophobic regions to water, thereby enhancing the overall binding affinity. This aligns with Yang *et al.* (2004), who reported that the interaction between calmodulin (CaM) and the smooth muscle myosin light chain kinase (smMLCK) peptide is largely driven by hydrophobic forces. These interactions create significant conformational strain in both the calmodulin protein and the smMLCK peptide. Notable, O'Neil *et al.* (1990) earlier reported that CaM was commonly found to interact with the protein partners through regions of positive charge, hydrophilic residues, and hydrophobicity in the helices.

However, the study, with a binding free energy of -11 kcal/mol, reveals that the hydrophobic contacts do not fully compensate for the conformational strain associated with binding. Similarly, in this study, the CaM-CBM complex exhibits a binding free energy of -6.2 kcal/mol, which, although indicative of a relatively strong binding interaction, remains moderate compared to the stronger binding energies typically associated with extensive hydrophobic forces. This comparison underscores the complexity of these interactions, where hydrophobic effects are balanced by the costs linked to conformational changes, ultimately resulting in a moderately favorable binding free energy in both systems.

Based on Fig. (5), the map of interactions emphasizes the critical role of the IL motif in stabilizing the interaction between Pk-CaM and Pk-CBM, revealing a nuanced balance of hydrophobic and polar forces. In the wild-type complex (CaM-CBM), the binding affinity of -6.2 kcal/mol is primarily driven by hydrophobic interactions facilitated by the IL motif. This suggests that the motif is essential for minimizing solvent exposure of

nonpolar regions, thereby enhancing the complex's stability. Soares *et al.* (2003) indicated that the removal of water molecules through hydration leads to the structural stability of the proteins. When the IL motif is removed in CaM-Var1, the interaction shifts to being dominated by hydrogen bonds, resulting in a stronger binding affinity of -8.0 kcal/mol. This improvement likely reflects the ability of hydrogen bonds to compensate for the loss of hydrophobic interactions by creating more specific and directional polar contacts.

Interestingly, substituting the IL motif with the ND motif in CaM-Var3 also strengthens hydrogen bonding interactions but results in a slightly lower binding affinity (-6.8 kcal/mol) compared to CaM-Var1. This difference suggests that although hydrogen bonds are significant contributors to stability, the IL motif provides a unique structural advantage that cannot be fully accommodated by polar substitutions. The IL motif may also play a role in maintaining the structural integrity of the binding interface, which could explain the comparatively lower binding affinities observed when it is altered or removed. In CBM with IQ motif, hydrophobic interaction was also reported to be the dominant and detrimental interaction mode for CaM (Fallon *et al.*, 2005).

In contrast, the IR motif appears to be less critical for binding. Removing it in CaM-Var2 or replacing it with the NA motif in CaM-Var4 results in weaker binding affinities of -5.4 kcal/mol and -5.3 kcal/mol, respectively. These values, which are lower than the wild-type CaM-CBM binding affinity, indicate that while the IR motif contributes to the interaction, it does not play as pivotal a role as the IL motif. The balance of hydrophobic and hydrogen bonding interactions observed in CaM-Var2 suggests that both interaction types are equally significant in this context. In comparison, the dominance of hydrogen bonds in CaM-Var4 highlights how polar contacts alone cannot fully compensate for the loss of the IR motif's contributions.

These findings collectively underscore the functional importance of the IL motif in achieving optimal binding affinity between Pk-CaM and Pk-CBM. The motif appears to serve a dual role, which are contributing to hydrophobic interactions that stabilize the binding interface and supporting the structural conformation necessary for effective complex formation. The IR motif, while less influential, enhances binding strength through secondary stabilization effects. This Analysis demonstrates how specific sequence motifs govern the interplay of hydrophobic and polar interactions, tailoring the binding affinity and specificity of the complex. However, while these *in silico* experiments provide valuable insights and predictions regarding molecular interactions of Pk-CBM and Pk-CaM, it is essential to conduct *in vitro* experiments to verify and confirm these predictions.

The findings from *in vitro* Analysis, including CD spectroscopy and the ANS fluorescence assay, provide

valuable insights into the interactions between calmodulin (CaM) and the Pk-CBM peptide. The alterations observed in the CD spectra (Fig. 7) indicate that binding with the CBM peptide induces significant changes in the secondary structure of Pk-CaM. This suggests that the interaction is more than just a physical attachment; it may also influence the functional properties of the protein. The role of calcium ions is crucial in these changes, as they activate Pk-CaM and modulate its interactions with various ligands. Earlier, Léger *et al.* (2022) implied that the Ca-bound form of CaM is an active form for binding to the effector proteins.

In the fluorescence assay (Fig. 8), the strong binding of ANS to Pk-CaM in the absence of the Pk-CBM peptide is evident, as indicated by the high fluorescence intensity. Principally, ANS occupied hydrophobic regions of the protein target, as outlined by Guliyeva and Gasymov (2020). This suggests that the hydrophobic regions of Pk-CaM are accessible for ANS binding, indicating that the protein's hydrophobic core is exposed to the solvent and capable of interacting with nonpolar molecules. However, the substantial decrease in fluorescence intensity upon the introduction of the Pk-CBM peptide demonstrates a competitive binding scenario. This suggests that the Pk-CBM peptide interacts with the same hydrophobic sites on Pk-CaM, effectively displacing ANS and reducing its binding affinity. The reduction in fluorescence intensity is a clear indication that the Pk-CBM peptide competes for binding to these hydrophobic sites, thus preventing the ANS probe from binding as efficiently. This observation aligns with the *in silico* interaction map, where the binding interface between Pk-CaM and Pk-CBM is predominantly dominated by hydrophobic regions. Together, these results reinforce the conclusion that hydrophobic interactions play a central role in the binding affinity between Pk-CaM and Pk-CBM while also providing insight into the competitive nature of this interaction. This competitive interaction implies that Pk-CBM effectively modulates the structural dynamics of Pk-CaM, which could have important implications for its physiological functions.

The estimated dissociation constant (Kd) of 54.8 μM , obtained from CD spectroscopy, can be compared to the *in silico* Kd value of 28 μM . This indicates that the experimental value is approximately two times higher than the computational value. However, it is important to note that these are two different methods for determining the Kd, each with its own inherent limitations and assumptions. Despite this discrepancy, both the experimental and computational results are in reasonable agreement and confirm the binding affinity between Pk-CaM and Pk-CBM. Additionally, the qualitative results from the ANS fluorescence assay further support this binding interaction. The assay revealed significant changes in fluorescence intensity upon the addition of Pk-

CBM, which is consistent with binding events that cause alterations in the environment of the ANS probe. These findings collectively provide strong evidence for the binding between Pk-CaM and Pk-CBM, reinforcing the conclusions drawn from both the Kd measurements and the fluorescence assay.

Conclusion

The current study confirmed the binding interaction between Pk-CaM and Pk-CBM through both *in silico* and *in vitro* assays. The *in silico* binding Analysis revealed several key findings. First, the structural model of Pk-CaM closely resembles canonical calmodulin, characterized by its helical configuration and calcium-binding EF-hand motifs. Second, the binding between Pk-CaM and Pk-CBM is driven by strong binding affinities, making the interaction energetically favorable and stable during the 100 ns simulation. Third, the interaction maps highlighted the pivotal role of specific residues, particularly Phe29 and the IL motif, in facilitating effective binding. In addition, circular dichroism and ANS fluorescence assays further confirmed the binding event, showing significant alterations in the secondary structure of Pk-CaM upon binding with the CBM peptide. These findings offer valuable insights into the potential role of Pk-FKBP35 in the Pk-CaM-mediated calcium signaling pathway based on their interconnected network.

Acknowledgment

The authors would like to thank Anna Robreth @ Roberth for critical input on the manuscript. We also extend our gratitude to Universiti Malaysia Sabah for its financial support (SPB0003-2020).

Funding Information

This research was funded by Universiti Malaysia Sabah under Skim Penyelidikan Berimpak (SPB0003-2020). The authors also acknowledge the partial support of Grant AFHO-00267 for this study.

Author's Contributions

Sazlinawatie Aladin: Conceptualization, data curation, investigation, and preparation of the manuscript.

Cahyo Budiman: Methodology, supervision, the author of the idea, head of the event, generalization, preparation of the manuscript, and final revision of the article.

Rafida Razali: Review, data curation, and editing manuscript.

Muhamad Arifin: Data curation on fluorescence spectroscopy, review and editing the final draft of the manuscript.

Ethics

The authors declare that they have no competitors' interests.

References

- Adiyoga, R., Arief, I. I., Budiman, C., & Abidin, A. (2022). In vitro anticancer potentials of *Lactobacillus plantarum* IIA-1A5 and *Lactobacillus acidophilus* IIA-2B4 extracts against WiDr human colon cancer cell line. *Food Sciences and Technology*, 42: e87221. <https://doi.org/10.1590/fst.87221>
- Alag, R., Bharatham, N., Dong, A., Hills, T., Harikishore, A., Widjaja, A. A., Shochat, S. G., Hui, R., & Yoon, H. S. (2009). Crystallographic structure of the tetratricopeptide repeat domain of *Plasmodium falciparum* FKBP35 and its molecular interaction with Hsp90 C-terminal pentapeptide. *Protein Science*, 18(10), 2115–2124. <https://doi.org/10.1002/pro.226>
- Afiyah, D. N., Arief, I. I., & Budiman, C. (2015). Proteolytic Characterization of Trimmed Beef Fermented Sausages Inoculated by Indonesian Probiotics: *Lactobacillus plantarum* IIA-2C12 and *Lactobacillus acidophilus* IIA-2B4. *Advance Journal of Food Science and Technology*, 8(1), 27–35. <https://doi.org/10.19026/ajfst.8.1459>
- Amir, A., Cheong, F. W., de Silva, J. R., Liew, J. W. K., & Lau, Y. L. (2018). *Plasmodium knowlesi* malaria: current research perspectives. *Infection and Drug Resistance*, 11, 1145–1155. <https://doi.org/10.2147/idr.s148664>
- Andrews, C., Xu, Y., Kirberger, M., & Yang, J. J. (2020). Structural Aspects and Prediction of Calmodulin-Binding Proteins. *International Journal of Molecular Sciences*, 22(1), 308. <https://doi.org/10.3390/ijms22010308>
- Aslanzadeh, V., & Ghaderia, M. (2012). Homology Modeling and Functional Characterization of PR-1a Protein of *Hordeum vulgare* subsp. *Vulgare*. *Bioinformatics*, 8(17), 807–811. <https://doi.org/10.6026/97320630008807>
- Au, S. X., Mohd Padzil, A., Muhd Noor, N. D., Matsumura, H., Raja Abdul Rahman, R. N. Z., & Normi, Y. M. (2023). Probing the substrate binding modes and catalytic mechanisms of BLEG-1, a promiscuous B3 metallo- β -lactamase with glyoxalase II properties. *PLOS ONE*, 18(9), e0291012. <https://doi.org/10.1371/journal.pone.0291012>
- Bähler, M., & Rhoads, A. (2002). Calmodulin signaling via the IQ motif. *FEBS Letters*, 513(1), 107–113. [https://doi.org/10.1016/s0014-5793\(01\)03239-2](https://doi.org/10.1016/s0014-5793(01)03239-2)
- Biasini, M., Bienert, S., Waterhouse, A., Arnold, K., Studer, G., Schmidt, T., Kiefer, F., Cassarino, T. G., Bertoni, M., Bordoli, L., & Schwede, T. (2014). SWISS-MODEL: modelling protein tertiary and quaternary structure using evolutionary information. *Nucleic Acids Research*, 42(W1), W252–W258. <https://doi.org/10.1093/nar/gku340>
- Budiman, C., Bando, K., Angkawidjaja, C., Koga, Y., Takano, K., & Kanaya, S. (2009). Engineering of monomeric FK506-binding protein 22 with peptidyl prolyl *cis-trans* isomerase. *The FEBS Journal*, 276(15), 4091–4101. <https://doi.org/10.1111/j.1742-4658.2009.07116.x>
- Budiman, C., Koga, Y., Takano, K., & Kanaya, S. (2011). FK506-Binding Protein 22 from a Psychrophilic Bacterium, a Cold Shock-Inducible Peptidyl Prolyl Isomerase with the Ability to Assist in Protein Folding. *International Journal of Molecular Sciences*, 12(8), 5261–5284. <https://doi.org/10.3390/ijms12085261>
- Budiman, C., Tadokoro, T., Angkawidjaja, C., Koga, Y., & Kanaya, S. (2012). Role of polar and nonpolar residues at the active site for PPIase activity of FKBP22 from *Shewanella* sp. SIB1. *The FEBS Journal*, 279(6), 976–986. <https://doi.org/10.1111/j.1742-4658.2012.08483.x>
- Chen, V. B., Arendall, W. B., Headd, J. J., Keedy, D. A., Immormino, R. M., Kapral, G. J., Murray, L. W., Richardson, J. S., & Richardson, D. C. (2012). MolProbity: all-atom structure validation for macromolecular crystallography. *International Tables for Crystallography*, 694–701. <https://doi.org/10.1107/97809553602060000884>
- Cheng, X., & Ivanov, I. (2012). Molecular dynamics. *Computational Toxicology: Volume 1, I*, 243–285. https://doi.org/10.1007/978-1-62703-050-2_11
- Chin, A. Z., Maluda, M. C. M., Jelip, J., Jeffrey, M. S. B., Culleton, R., & Ahmed, K. (2020). Malaria elimination in Malaysia and the rising threat of *Plasmodium knowlesi*. *Journal of Physiological Anthropology*, 39(1), 36. <https://doi.org/10.1186/s40101-020-00247-5>
- de Oliveira, L. S., Alborghetti, M. R., Carneiro, R. G., Bastos, I. M. D., Amino, R., Grellier, P., & Charneau, S. (2021). Calcium in the Backstage of Malaria Parasite Biology. *Frontiers in Cellular and Infection Microbiology*, 11, 708834. <https://doi.org/10.3389/fcimb.2021.708834>
- Dominguez, C., Boelens, R., & Bonvin, A. M. J. J. (2003). HADDOCK: A Protein–Protein Docking Approach Based on Biochemical or Biophysical Information. *Journal of the American Chemical Society*, 125(7), 1731–1737. <https://doi.org/10.1021/ja026939x>

- Dürvanger, Z., Juhász, T., Liliom, K., & Harmat, V. (2023). Structures of calmodulin–melittin complexes show multiple binding modes lacking classical anchoring interactions. *Journal of Biological Chemistry*, 299(4), 104596. <https://doi.org/10.1016/j.jbc.2023.104596>
- Fallon, J. L., Halling, D. B., Hamilton, S. L., & Quioco, F. A. (2005). Structure of Calmodulin Bound to the Hydrophobic IQ Domain of the Cardiac Cav1.2 Calcium Channel. *Structure*, 13(12), 1881–1886. <https://doi.org/10.1016/j.str.2005.09.021>
- Goh, C. K. W., Silvester, J., Wan Mahadi, W. N. S., Chin, L. P., Ying, L. T., Leow, T. C., Kurahashi, R., Takano, K., & Budiman, C. (2018). Expression and characterization of functional domains of FK506-binding protein 35 from *Plasmodium knowlesi*. *Protein Engineering, Design and Selection*, 31(12), 489–498. <https://doi.org/10.1093/protein/gzz008>
- Guliyeva, A. J., & Gasymov, O. K. (2020). ANS fluorescence: Potential to discriminate hydrophobic sites of proteins in solid states. *Biochemistry and Biophysics Reports*, 24, 100843. <https://doi.org/10.1016/j.bbrep.2020.100843>
- Horváth, I., Harmat, V., Perczel, A., Pálfi, V., Nyitray, L., Nagy, A., Hlavanda, E., Náráy-Szabó, G., & Ovádi, J. (2005). The Structure of the Complex of Calmodulin with KAR-2. *Journal of Biological Chemistry*, 280(9), 8266–8274. <https://doi.org/10.1074/jbc.m410353200>
- Huff, C. G. (1972). The Primate Malarias. *The American Journal of Tropical Medicine and Hygiene*, 21(5), 602–603. <https://doi.org/10.4269/ajtmh.1972.21.602>
- Illang, N. I., Lee, P.-C., Kamaruzaman, K. A., & Budiman, C. (2023). Inhibition properties of collagen hydrolysates against FKBP35 of *Plasmodium knowlesi*. *Malaysian Journal of Microbiology*, 19(6), 727–734. <https://doi.org/10.21161/mjm.230021>
- Jensen, D., Reynolds, N., Yang, Y.-P., Shakya, S., Wang, Z.-Q., Stuehr, D. J., & Wei, C.-C. (2015). The exchanged EF-hands in calmodulin and troponin C chimeras impair the Ca²⁺-induced hydrophobicity and alter the interaction with Orail1: a spectroscopic, thermodynamic and kinetic study. *BMC Biochemistry*, 16(1), 6. <https://doi.org/10.1186/s12858-015-0036-7>
- Kia, K. W., Arief, I. I., Sumantri, C., & Budiman, C. (2015). Plantaricin IIA-1A5 from *Lactobacillus plantarum* IIA-1A5 Retards Pathogenic Bacteria in Beef Meatball Stored at Room Temperature. *American Journal of Food Technology*, 11(1–2), 37–43. <https://doi.org/10.3923/ajft.2016.37.43>
- Kumar, S. P., Girija, A. S. S., & Priyadharsini, J. V. (2020). Targeting NM23-H1-mediated Inhibition of Tumour Metastasis in Viral Hepatitis with Bioactive Compounds from *Ganoderma lucidum*: A Computational Study. *Indian Journal of Pharmaceutical Sciences*, 82(2), 300–305. <https://doi.org/10.36468/pharmaceutical-sciences.650>
- Kumari, P., Kumar, M., Sehgal, N., & Aggarwal, N. (2022). *In silico* Analysis of kiss2, expression studies and protein–protein interaction with gonadotropin-releasing hormone 2 (GnRH2) and luteinizing hormone beta (LHβ) in *Heteropneustes fossilis*. *Journal of Biomolecular Structure and Dynamics*, 40(10), 4543–4557. <https://doi.org/10.1080/07391102.2020.1860820>
- LaCount, D. J., Vignali, M., Chettier, R., Phansalkar, A., Bell, R., Hesselberth, J. R., Schoenfeld, L. W., Ota, I., Sahasrabudhe, S., Kurschner, C., Fields, S., & Hughes, R. E. (2005). A protein interaction network of the malaria parasite *Plasmodium falciparum*. *Nature*, 438(7064), 103–107. <https://doi.org/10.1038/nature04104>
- Laemmli, U. K. (1970). Cleavage of Structural Proteins during the Assembly of the Head of Bacteriophage T4. In *Nature* (Vol. 227, Issue 5259, pp. 680–685). <https://doi.org/10.1038/227680a0>
- Laskowski, R. A., & Swindells, M. B. (2011). LigPlot+: Multiple Ligand–Protein Interaction Diagrams for Drug Discovery. *Journal of Chemical Information and Modeling*, 51(10), 2778–2786. <https://doi.org/10.1021/ci200227u>
- Laskowski, R. A., MacArthur, M. W., & Thornton, J. M. (2012). PROCHECK: validation of protein-structure coordinates. *International Tables for Crystallography*, 684–687. <https://doi.org/10.1107/97809553602060000882>
- Laskowski, R. A., MacArthur, M. W., Moss, D. S., & Thornton, J. M. (1993). PROCHECK: A Program to Check the Stereochemical Quality of Protein Structures. *Journal of Applied Crystallography*, 26(2), 283–291. <https://doi.org/10.1107/s0021889892009944>
- Léger, C., Pitard, I., Sadi, M., Carvalho, N., Brier, S., Mechaly, A., Raoux-Barbot, D., Davi, M., Hoos, S., Weber, P., Vachette, P., Durand, D., Haouz, A., Guijarro, J. I., Ladant, D., & Chenal, A. (2022). Dynamics and structural changes of calmodulin upon interaction with the antagonist calmidazolium. *BMC Biology*, 20(1), 176. <https://doi.org/10.1186/s12915-022-01381-5>

- Lindang, H.U., & Budiman, C. (2022). Structural and substrate interaction properties of alkaline phosphatase from *Paenibacillus* sp. PSB04: In-Silico Analysis. *OnLine Journal of Biological Sciences*, 22(3), 256-267.
<https://doi.org/10.3844/ojbsci.2022.256.267>
- Lovell, S. C., Davis, I. W., Arendall, W. B., de Bakker, P. I. W., Word, J. M., Prisant, M. G., Richardson, J. S., & Richardson, D. C. (2003). Structure validation by C α geometry: ϕ , ψ and C β deviation. *Proteins: Structure, Function and Bioinformatics*, 50(3), 437–450.
<https://doi.org/10.1002/prot.10286>
- Lüthy, R., Bowie, J. U., & Eisenberg, D. (1992). Assessment of protein models with three-dimensional profiles. *Nature*, 356(6364), 83–85.
<https://doi.org/10.1038/356083a0>
- Millar, S. B., & Cox-Singh, J. (2015). Human infections with *Plasmodium knowlesi* zoonotic malaria. *Clinical Microbiology and Infection*, 21(7), 640–648.
<https://doi.org/10.1016/j.cmi.2015.03.017>
- Mollazadeh, S., Keyvanfar, H., Bakhshesh, M., & Nikbakht Brujeni, G. (2022). Epitope Identification in BEFV N protein for Detecting Effective Points. *Journal of Advanced Biomedical Sciences*.
<https://doi.org/10.18502/jabs.v12i1.8875>
- Monaghan, P., & Bell, A. (2005). A *Plasmodium falciparum* FK506-binding protein (FKBP) with peptidyl–prolyl cis–trans isomerase and chaperone activities. *Molecular and Biochemical Parasitology*, 139(2), 185–195.
<https://doi.org/10.1016/j.molbiopara.2004.10.007>
- Monaghan, P., Fardis, M., Revill, W. P., & Bell, A. (2005). Antimalarial Effects of Macrolactones Related to FK520 (Ascomycin) Are Independent of the Immunosuppressive Properties of the Compounds. *The Journal of Infectious Diseases*, 191(8), 1342–1349. <https://doi.org/10.1086/428454>
- Monaghan, P., Leneghan, D. B., Shaw, W., & Bell, A. (2017). The antimalarial action of FK506 and rapamycin: evidence for a direct effect on FK506-binding protein PfFKBP35. *Parasitology*, 144(7), 869–876.
<https://doi.org/10.1017/s0031182017000245>
- O’Neil, K. T., & DeGrado, W. F. (1990). How calmodulin binds its targets: sequence independent recognition of amphiphilic α -helices. *Trends in Biochemical Sciences*, 15(2), 59–64.
[https://doi.org/10.1016/0968-0004\(90\)90177-d](https://doi.org/10.1016/0968-0004(90)90177-d)
- Parikesit, A. A., & Nurdiansyah, R. (2021). Natural products repurposing of the H5N1-based lead compounds for the most fit inhibitors against 3C-like protease of SARS-CoV-2. *Journal of Pharmacy & Pharmacognosy Research*, 9(5), 730–745.
https://doi.org/10.56499/jppres21.1080_9.5.730
- Park, S. W., Lee, B. H., Song, S. H., & Kim, M. K. (2023). Revisiting the Ramachandran plot based on statistical Analysis of static and dynamic characteristics of protein structures. *Journal of Structural Biology*, 215(1), 107939.
<https://doi.org/10.1016/j.jsb.2023.107939>
- Rhoads, A. R., & Friedberg, F. (1997). Sequence motifs for calmodulin recognition. *The FASEB Journal*, 11(5), 331–340.
<https://doi.org/10.1096/fasebj.11.5.9141499>
- Robert, A. R., Aladin, S., Budiman, C., Chin, L. P., Kamaruzzaman, K. A., Leow, T. C., & Padzil, A. M. (2023). Heterologous expression and purification of calmodulin from *Plasmodium knowlesi* using codon-optimized synthetic gene. *Malaysian Journal of Microbiology*, 19(6), 718–726.
<https://doi.org/10.21161/mjm.230020>
- Silvester, J., Anak Linda, H. U., Chin, L. P., Ying, L. T., & Budiman, C. (2017). Structure and Molecular Dynamic Regulation of FKBP35 from *Plasmodium knowlesi* by Structural Homology Modeling and Electron Microscopy. *Journal of Biological Sciences*, 17(8), 369–380.
<https://doi.org/10.3923/jbs.2017.369.380>
- Singh, B., & Daneshvar, C. (2013). Human Infections and Detection of *Plasmodium knowlesi*. *Clinical Microbiology Reviews*, 26(2), 165–184.
<https://doi.org/10.1128/cmr.00079-12>
- Siraj, M. A., Rahman, Md., Tan, G., & Seidel, V. (2021). Molecular Docking and Molecular Dynamics Simulation Studies of Triterpenes from *Vernonia patula* with the Cannabinoid Type 1 Receptor. *International Journal of Molecular Sciences*, 22(7), 3595. <https://doi.org/10.3390/ijms22073595>
- Soares, C. M., Teixeira, V. H., & Baptista, A. M. (2003). Protein Structure and Dynamics in Nonaqueous Solvents: Insights from Molecular Dynamics Simulation Studies. *Biophysical Journal*, 84(3), 1628–1641. [https://doi.org/10.1016/s0006-3495\(03\)74972-8](https://doi.org/10.1016/s0006-3495(03)74972-8)
- Studer, G., Rempfer, C., Waterhouse, A. M., Gumienny, R., Haas, J., & Schwede, T. (2020). QMEANDisCo—distance constraints applied on model quality estimation. *Bioinformatics*, 36(6), 1765–1771.
<https://doi.org/10.1093/bioinformatics/btz828>
- Swargiary, A., Mahmud, S., & Saleh, Md. A. (2022). Screening of phytochemicals as potent inhibitor of 3-chymotrypsin and papain-like proteases of SARS-CoV2: an *in silico* approach to combat COVID-19. *Journal of Biomolecular Structure and Dynamics*, 40(5), 2067–2081.
<https://doi.org/10.1080/07391102.2020.1835729>

- Tung, T. H. (2010). Tacrolimus (FK506): Safety and applications in reconstructive surgery. *Hand*, 5(1), 1–8. <https://doi.org/10.1007/s11552-009-9193-8>
- Van Zundert, G. C. P., Rodrigues, J. P. G. L. M., Trellet, M., Schmitz, C., Kastiris, P. L., Karaca, E., Melquiond, A. S. J., van Dijk, M., de Vries, S. J., & Bonvin, A. M. J. J. (2016). The HADDOCK2.2 Web Server: User-Friendly Integrative Modeling of Biomolecular Complexes. *Journal of Molecular Biology*, 428(4), 720–725. <https://doi.org/10.1016/j.jmb.2015.09.014>
- Waterhouse, A., Bertoni, M., Bienert, S., Studer, G., Tauriello, G., Gumienny, R., Heer, F. T., de Beer, T. A. P., Rempfer, C., Bordoli, L., Lepore, R., & Schwede, T. (2018). SWISS-MODEL: Homology Modelling of Protein Structures and Complexes. *Nucleic Acids Research*, 46(W1), W296–W303. <https://doi.org/10.1093/nar/gky427>
- World Health Organization. (2022). *World malaria report 2022*.
- Yang, C., Jas, G. S., & Kuczera, K. (2004). Structure, dynamics and interaction with kinase targets: computer simulations of calmodulin. *Biochimica et Biophysica Acta (BBA) - Proteins and Proteomics*, 1697(1–2), 289–300. <https://doi.org/10.1016/j.bbapap.2003.11.032>
- Yoon, H. R., Kang, C. B., Chia, J., Tang, K., & Yoon, H. S. (2007). Expression, purification and molecular characterization of *Plasmodium falciparum* FK506-binding protein 35 (PFKBP35). *Protein Expression and Purification*, 53(1), 179–185. <https://doi.org/10.1016/j.pep.2006.12.019>
- Zhang, M., Abrams, C., Wang, L., Gizzi, A., He, L., Lin, R., Chen, Y., Loll, P. J., Pascal, J. M., & Zhang, J. (2012). Structural Basis for Calmodulin as a Dynamic Calcium Sensor. *Structure*, 20(5), 911–923. <https://doi.org/10.1016/j.str.2012.03.019>